Journal of Environmental Management 393 (2025) 127004

Contents lists available at ScienceDirect

Journal of Environmental Management

journal homepage: www.elsevier.com/locate/jenvman

Research article

Removal of meropenem from hospital wastewater using biochar derived from grape stalks

José L.S. Duarte [a], Ana Hayat [a], Mario de la Fuente [b], Carmen M. Domínguez [a], Aurora Santos [a], Salvador Cotillas [a,*]

[a] Department of Chemical and Materials Engineering, Faculty of Chemical Sciences, Complutense University of Madrid, Avenida Complutense s/n, 28040, Madrid, Spain
[b] Department of Agricultural Production, School of Agronomy, Food and Biosystems Engineering, Polytechnic University of Madrid, Ciudad Universitaria, 28040, Madrid, Spain

ARTICLE INFO

Keywords:
Biochar
Grape residues
Meropenem
Hospital wastewater
Adsorption

ABSTRACT

This study focuses on synthesizing biochar from grape stalks and its application for removing the antibiotic meropenem (MRP) from aqueous solutions. The raw biochar was chemically activated with NaOH under mild conditions and thoroughly characterized to elucidate its adsorption mechanisms. Preliminary tests confirmed the need for activation to enhance the adsorption efficiency. The effect of initial MRP concentration, biochar dosage, solution pH, kinetics, and equilibrium were investigated. Furthermore, the adsorption of MRP contained in simulated hospital wastewater (HWW) was also evaluated. Characterization revealed a honeycomb pore structure, high mineral content, and surface functional groups relevant for adsorption. Kinetic data fitted the pseudo-second-order model, and equilibrium isotherms fitted the Freundlich model. Thermodynamic analysis indicated spontaneous adsorption in ultrapure water, with an enhanced spontaneity observed in HWW due to the presence of competing ions. Desorption tests showed 90 % MRP removal after five cycles. In simulated HWW, the activated biochar achieved complete MRP removal at low (5 mg dm^{-3}) and high (100 mg dm^{-3}) concentrations and concurrently reduced salinity. The maximum adsorption capacity (80 mg g^{-1}) was reached at an initial concentration of 100 mg dm^{-3}, under optimal conditions of pH 3 and 1.0 g dm^{-3} of biochar. These findings highlight the potential of grape stalk-derived biochar as an effective and reusable adsorbent for hospital wastewater treatment.

1. Introduction

The emergence of antibiotic-resistant bacteria (ARB) has become a critical concern to the scientific community. This phenomenon stems from the interaction between pathogenic microorganisms and residual pharmaceuticals in the environment, facilitating the acquisition and spread of resistance genes (Cotillas et al., 2018; Herraiz-Carboné et al., 2021; Moratalla et al., 2022). Hospitals are considered epicenters of this issue, discharging between 200 and 1200 dm^3 of wastewater per bed per day, depending on the country's economic status (Al Aukidy et al., 2018; Verlicchi, 2021). Their effluents contain a complex mixture of hazardous substances from medical procedures, laboratory analyses, research activities, and patient excreta. These pollutants pose significant risks to human health and aquatic ecosystems, even at trace concentrations. Furthermore, hospital wastewater often contains unmetabolized pharmaceuticals and their transformation products (Hayat et al., 2025). Fourth-generation antibiotics, designed to combat ARB, are of particular concern, as they are now extensively used in clinical practice worldwide (Pham et al., 2022).

Meropenem (MRP) is a carbapenem-class β-lactam antibiotic characterized by its broad-spectrum activity against Gram-positive and Gram-negative bacteria, including *Pseudomonas aeruginosa* and anaerobic species when administered intravenously. It exerts its bactericidal effect by inhibiting cell wall synthesis, leading to osmotic lysis and cell death. A major advantage of MRP is its stability against a wide array of β-lactamases that inactivate many other β-lactam antibiotics. Furthermore, MRP is highly recalcitrant to biological degradation and readily passes through conventional wastewater treatment systems. As one of the last-resort agents for infections caused by ARB, particularly in intensive care settings, its clinical use has surged in both human and veterinary medicine (Kordestani et al., 2020; Pham et al., 2022). However, this increased usage has led to detectable concentrations of MRP in

* Corresponding author.
E-mail address: salvacot@ucm.es (S. Cotillas).

https://doi.org/10.1016/j.jenvman.2025.127004
Received 17 May 2025; Received in revised form 29 July 2025; Accepted 14 August 2025
Available online 18 August 2025

aquatic environments, where even trace levels can disrupt microbial communities and pose human health risks. Therefore, efficiently removing MRP from wastewater before its release into natural ecosystems is essential to mitigate the spread of emerging contaminants and protect the ecosystem and public health (Ahmadi et al., 2020; Moratalla et al., 2022).

Adsorption has emerged as a highly effective and versatile technology for water treatment, prized for its operational simplicity, economic viability, and potential for adsorbent regeneration. Its ability to sequester various contaminants, from dissolved organics to trace pharmaceuticals, makes it an attractive complement or alternative to more complex treatment schemes (da Silva Santos et al., 2021; Sepúlveda et al., 2021). However, adsorption performance hinges critically on the physicochemical properties of the adsorbent material, including its surface area, porosity, functional groups, and stability. Identifying and developing highly efficient adsorbents remains a critical challenge in optimizing adsorption-based treatment processes (Hai Nguyen Tran et al., 2017).

Within the framework of a circular economy, valorizing lignocellulosic residues as low-cost adsorbents has gained increasing attention as it aligns with the principles of sustainability, waste reduction, and resource efficiency. Agricultural and industrial byproducts, such as fruit pruning, sawdust, and husks, can be transformed into biochar or hydrochar, thereby diverting biomass from waste streams while producing value-added materials for pollutant removal (Bhatnagar and Sillanpää, 2010; Bulgariu et al., 2019; Lucaci et al., 2019). Recent advances in biochar modification strategies have significantly enhanced its adsorption capacity for contaminants. Techniques such as acid/base activation, impregnation with metal oxides, magnetic functionalization, and surface oxidation have been reported to increase porosity, surface area, and the abundance of reactive sites (Akkari et al., 2023; Georgin et al., 2022). Alkaline activation, in particular, has gained attention due to its ability to improve functional group availability and graphitization, contributing to more effective removal of pharmaceuticals from water matrices (Ghosh and Sahu, 2023; Zeghioud and Mouhamadou, 2023).

These bio-based sorbents have demonstrated impressive efficacy in capturing heavy metals, dyes, and emerging contaminants, including antibiotics, often matching or surpassing that of conventional carbonaceous adsorbents (Crini and Lichtfouse, 2019; Vasconcelos et al., 2023). Furthermore, coupling adsorption with other treatment technologies (advanced oxidation, membrane filtration …) enables more robust treatment trains to address complex wastewater matrices. Developing sustainable, high-performance adsorbents from lignocellulosic waste supports resource-efficient water purification and broader environmental stewardship goals.

Building on the foregoing, this study explores the adsorption of MRP contained in aqueous effluents using biochar derived from grape stalks. The lignocellulosic composition of the grape stalks used is this study can be similar to that of other grape residues from *Vitis vinifera* containing approximately 30–40 % cellulose, 20–30 % hemicellulose, and 25–35 % lignin, depending on the growing and harvesting conditions (da Silva et al., 2024; Georgin et al., 2022). This high lignin content contributes to the aromatic carbon framework of the resulting biochar, while the cellulose and hemicellulose fractions promote the formation of pores and functional groups upon pyrolysis. The raw biochar was synthesized and chemically activated with sodium hydroxide under mild conditions to enhance surface functionality and porosity. Comprehensive physicochemical characterization was conducted to elucidate the adsorptive properties of biochar. Batch experiments were then carried out to evaluate MRP removal: kinetics (fitting pseudo-first and pseudo-second-order models) and equilibrium isotherm tests (Langmuir and Freundlich) were performed to reveal the underlying adsorption mechanisms and capacity under varying pH, contact time, and adsorbent dosage. Additionally, regeneration potential was assessed through multiple desorption cycles, and adsorption performance was validated in simulated hospital wastewater to demonstrate the practical applicability and reusability of NaOH-activated grape stalk biochar for real-world treatment scenarios.

2. Materials and methods

2.1. Chemicals and material preparation

Grape stalks (GS) were collected from the agronomic experimentation field of the Polytechnic University of Madrid (Spain). The biomass was washed with tap water, oven-dried at 85 °C for 24 h, ground and pyrolyzed in a muffle furnace at 550 °C for 2 h (Shukla et al., 2024). The resulting biochar (BC) was sieved (<1.0 mm), washed four times with 50 % (v/v) ethanol (VWR), and a portion was chemically activated by stirring in 1.5 M NaOH (Fisher) for 2 h. The activated biochar (BCA) was rinsed with ultrapure water to neutral pH and dried (Akkari et al., 2023).

Simulated hospital wastewater (HWW) was prepared with reagent-grade salts (Table S1), including Na_2SO_4, NaCl, NH_4Cl, Na_3PO_4, $NaNO_3$, $CaCl_2$, $NaHCO_3$, $MgSO_4$, CH_3COONa, K_2SO_4, and urea (Hayat et al., 2025). All chemicals were purchased from Sigma Aldrich, Fisher, or Panreac.

2.2. Material characterization

Morphology and surface texture were analyzed using scanning electron microscopy (JEOL JSM 6335F). Functional groups were identified by FTIR (Nicolet iS50, ATR mode, 4000–400 cm^{-1}, 4 cm^{-1} resolution, 50 scans) and Raman spectroscopy (NT-MDT NTegra Spectra). Thermogravimetric and calorimetric analyses were conducted with TGA-DSC (TA SDT-Q600) under nitrogen (20 cm^3 min^{-1}) up to 1000 °C at 10 °C min^{-1}. X-ray diffraction (XRD) was performed with a Bruker D8 ADVANCE using Cu Kα radiation, scanned from 3° to 90° 2θ (0.02° steps). The point of zero charge (pH_{PZC}) was determined according to the procedure described in the literature (Henrique et al., 2020).

2.3. Experimental procedure

2.3.1. Adsorption preliminary studies

BC and BCA (5–80 mg) were contacted with MRP solutions (5–100 mg dm^{-3}) in ultrapure water to compare performance. The mixture (20 cm^3) was stirred at 150 rpm for 24 h at 25 °C in Teflon tubes. Detailed data supporting these preliminary comparisons are provided in the Supplementary Material (Table S3).

The adsorption capacity (q_t, mg g^{-1}) and removal efficiency (% removal) were calculated by equations (1) and (2), respectively.

$$q_t = \frac{(C_0 - C_t)}{m} \cdot V \quad (1)$$

$$\%\ \text{removal} = \frac{C_0 - C_t}{C_0} \cdot 100 \quad (2)$$

Where C_0 and C_t are the initial and equilibrium MRP concentrations (mg dm^{-3}), respectively, V is the volume (dm^3), and m is the adsorbent mass (g).

MRP was quantified by HPLC (Agilent 1100, DAD detector, 300 nm) using a Poroshell 120 EC-C18 column (3.0 × 150 mm, 2.7 μm) at 40 °C. The mobile phase was 0.1 % formic acid:acetonitrile (85:15 v/v), 0.3 cm^3 min^{-1} flow rate, and 20 μL injection volume (Kordestani et al., 2020).

2.3.2. Kinetics, equilibrium, and thermodynamics

Kinetic studies used BCA at 5 g dm^{-3} and MRP at 5, 50, and 100 mg dm^{-3}. Samples were taken at 10–240 min. The resulting data were fitted to the pseudo-first-order (PFO) (Eq. (3)) (Lagergren, 1898) and pseudo-second-order (PSO) models (Eq. (4)) (Ho and McKay, 1999).

$$q_t = q_e[1 - \exp(-k_1 * t)] \quad (3)$$

$$q_t = \frac{k_2 q_e^2 t}{1 + k_2 q_e t} \quad (4)$$

Where q_t (mg g^{-1}) is the amount adsorbed at time t (min), q_e (mg g^{-1}) is the equilibrium adsorption capacity, k_1 (min^{-1}) is the PFO rate constant, and k_2 (g mg^{-1} min^{-1}) is the PSO rate constant.

Equilibrium isotherms were performed at 30, 45, and 60 °C using 5–200 mg dm^{-3} of MRP with 5 g dm^{-3} BCA for 360 min. Models included Langmuir (Eq. (5)) (Langmuir, 1918), Freundlich (Eq. (6)) (Freundlich, 1906), Liu (Eq. (7)) (Liu et al., 2003) and Sips (Eq. (8)) (Sips, 1948).

$$q_e = \frac{q_{máx} K_L C_e}{1 + K_L C_e} \quad (5)$$

$$q_e = K_F C_e^{1/n} \quad (6)$$

$$q_e = \frac{q_L \cdot (K_L \cdot C_e)^{nL}}{1 + (K_L \cdot C_e)^{nL}} \quad (7)$$

$$q_e = \frac{q_S (k_S C_e)^{m_S}}{1 + (k_S C_e)^{m_S}} \quad (8)$$

where q_{max} (mg g^{-1}) is the maximum monolayer capacity, K_L (L mg^{-1}) is the Langmuir constant, C_e (mg dm^{-3}) is the equilibrium concentration, K_F [(mg dm^{-3})(dm^3 g^{-1})$^{1/n}$] is the Freundlich constant, and n is a constant related to the intensity of adsorption (−). q_L is the Liu maximum adsorption capacity (mg g^{-1}), K_{Liu} is the Liu equilibrium constant (L mg^{-1}); n_L is Liu model, respectively, (dimensionless); q_S is the maximum adsorption capacity from the Sips model (mg g^{-1}), K_{Sips} is the Sips constant (L mg^{-1}) and m_S is the exponent of the Sips model. Thermodynamic parameters (ΔG^0, ΔH^0, ΔS^0) were derived from Van't Hoff plots using equations (9)–(11).

$$\Delta G^0 = -RT\ln(K_e) \quad (9)$$

$$\Delta G^0 = \Delta H^0 - T\Delta S^0 \quad (10)$$

$$\ln(k_e) = \frac{\Delta S^0}{R} - \frac{\Delta H^0}{RT} \quad (11)$$

Where K_e (dm^3 mg^{-1}) is the equilibrium constant from the best-fit isotherm, R is the universal gas constant ($8.31 \cdot 10^{-3}$ kJ mol^{-1} K^{-1}), and T is the absolute temperature (K) (Sepúlveda et al., 2021).

2.3.3. Desorption-reusability and HWW matrix study

BCA (5 g dm^{-3}) was contacted with 50 mg dm^{-3} MRP for 24 h at 25 °C. After adsorption, BCA was filtered and desorbed with 0.1 M NaOH for 4 h, then rinsed and dried at 105 °C. Reusability was evaluated over five cycles. Adsorption tests were repeated in simulated HWW (Table S1). Residual MRP was measured by HPLC. Anions and cations were quantified by ion chromatography (Metrohm 930 Compact IC Flex), using Metrosep A Supp 5 (anions) and C6 (cations) columns with standard eluents and conductivity detection.

3. Results and discussion

3.1. Biochar characterization

Fig. 1 shows SEM images of BC and BCA, clearly illustrating the morphological transformations imparted by chemical activation. SEM revealed that NaOH activation transformed the surface morphology of the raw biochar (BC) into a more organized honeycomb-like structure with well-developed pores (Fig. 1a and b). This improved porosity is associated with enhanced surface accessibility and a higher number of active sites, as observed in the images of the activated biochar (BCA) (Fig. 1c and d) (Akkari et al., 2023; Georgin et al., 2022; Ghosh and Sahu, 2023).

FTIR spectra (Fig. 2a) confirmed the presence of functional groups critical for adsorption, including hydroxyl, carboxyl, and amine groups (see Table S2 for band assignments). The peak at 1415 cm^{-1} is

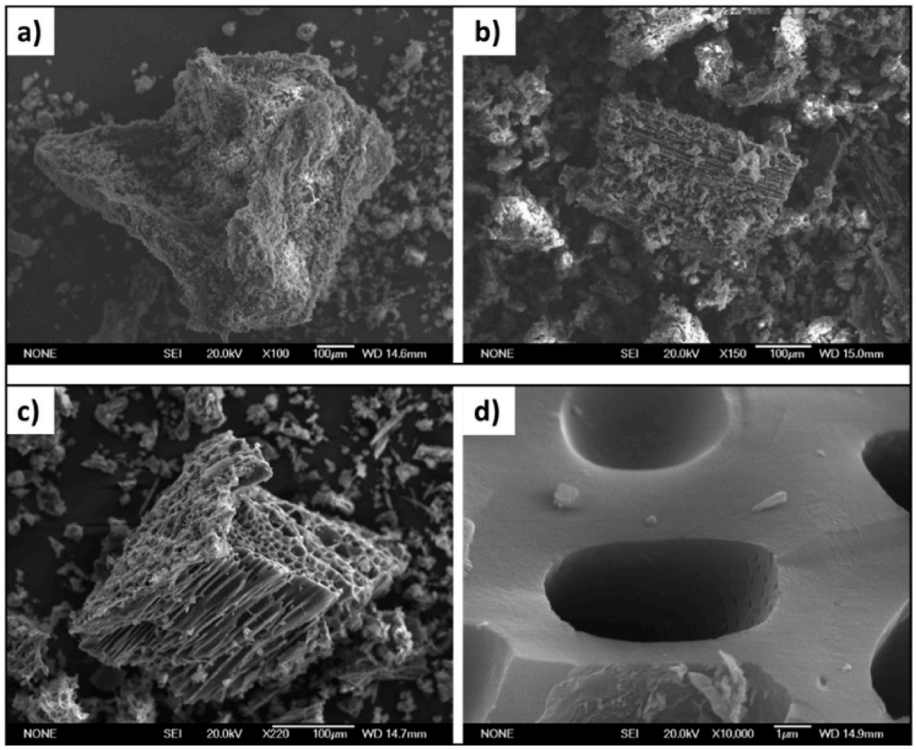

Fig. 1. – SEM images at different magnifications of BC (a) and (b) and BCA (c) and (d).

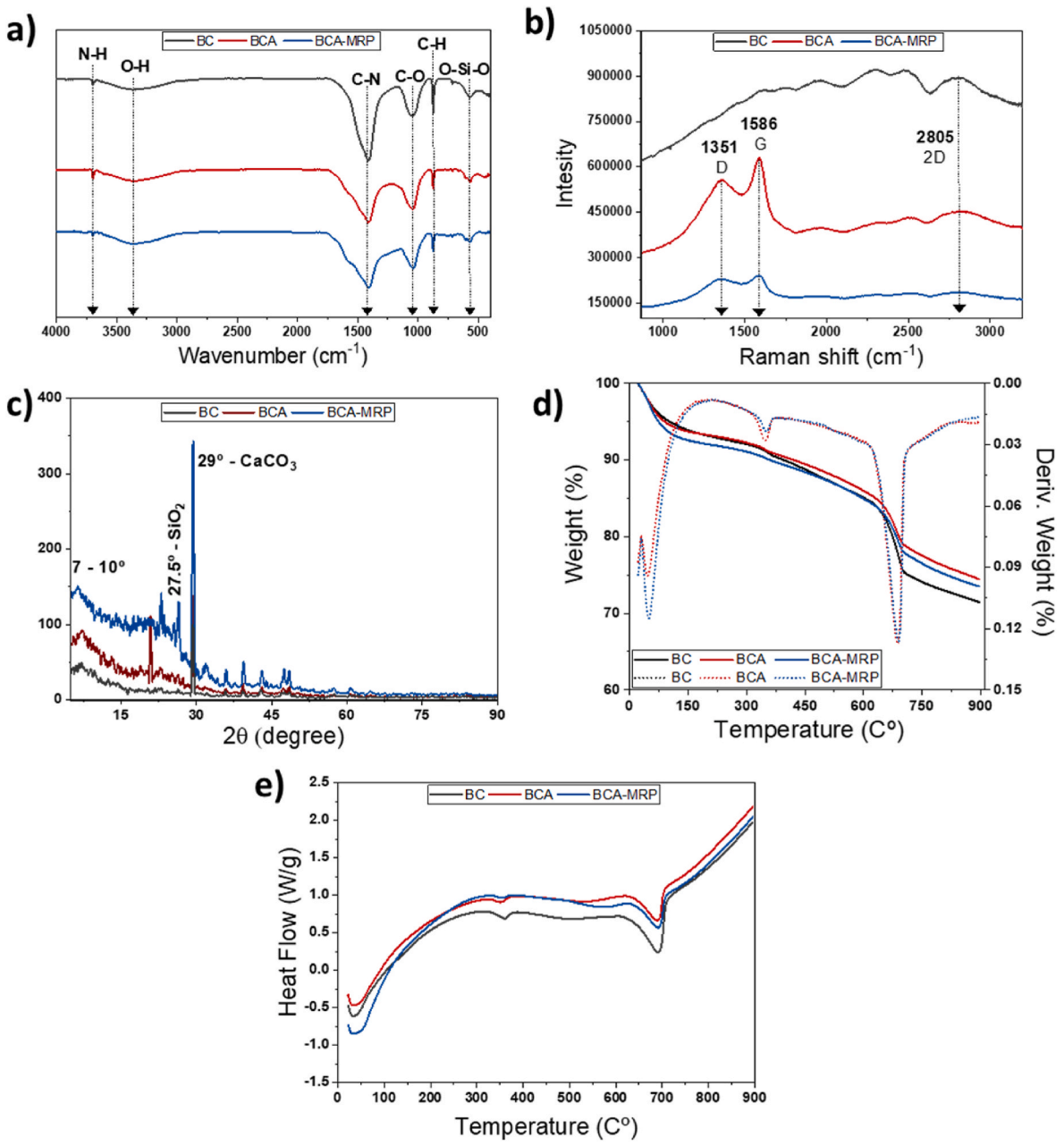

Fig. 2. – (a) FTIR spectra; (b) Raman spectra; (c) X-ray diffractograms (d) Thermogravimetric degradation curves; (e) DSC curves.

characteristic of C-N single bond vibrations (Lee, 2008; Majumdar et al., 2012), and the band at 1360 cm^{-1} arises from C–O stretching within lignin, cellulose, and hemicellulose moieties (da Silva et al., 2024). A deformation mode of phenyl C-H appears at 870 cm^{-1} (Akkari et al., 2023), and the signal at 570 cm^{-1} indicates O-Si-O vibrations from silica residues (Shukla et al., 2024). After activation, the BCA showed an increased intensity in N-H (3698 cm^{-1}) and O-H stretching bands (3425 and 3245 cm^{-1}), indicating surface enrichment in polar functionalities. These groups facilitate hydrogen bonding and electrostatic interactions with meropenem.

Raman analysis showed the appearance of defined D and G bands at 1351 and 1586 cm^{-1} in BCA, which were absent or poorly resolved in BC (Fig. 2b). The raw biochar (BC) spectrum is largely featureless, save for a faint 2D band around 2805 cm^{-1}, indicative of its highly disordered structure and heterogeneous mix of oxidized carbon species. These results suggest that activation improved the graphitic order of the carbon matrix, increasing structural uniformity and electronic delocalization, both favorable for π-π interactions with the antibiotic. The XRD patterns (Fig. 2c) revealed broad peaks associated with amorphous carbon and minor crystalline phases such as SiO_2 and $CaCO_3$. The presence of turbostratic carbon structures was evidenced by the peak near 22°, indicating partial graphitization. These features contribute to the hybrid character of the adsorbent, combining disordered and graphitic domains.

Thermogravimetric (TGA) and differential scanning calorimetry (DSC) analyses showed that BCA possesses high thermal stability, with three main degradation steps corresponding to moisture loss (<150 °C), decomposition of labile organics (150–600 °C), and carbonate decomposition (>600 °C). Compared to BC, BCA showed reduced mass loss in the mid-temperature range, indicating a more stable carbon matrix. The endothermic response of MRP-saturated BCA confirmed drug adsorption onto the material (Fig. 2d and e).

Overall, NaOH activation enhanced the physicochemical properties of grape-stalk-derived biochar by increasing porosity, introducing polar

surface groups, and improving carbon structural order. These modifications explain the high affinity of BCA for meropenem and its excellent performance in adsorption applications.

3.2. Adsorption studies

Batch experiments were conducted to evaluate the impact of NaOH activation on MRP adsorption performance. As shown in Fig. 3a, the raw biochar (BC) exhibited moderate removal efficiencies (48–60 %) across adsorbent dosages ranging from 0.25 to 5.0 g dm^{-3}, with no clear trend. Conversely, the activated biochar (BCA) consistently achieved higher removal (79–92 %) under the same conditions, confirming the effectiveness of the chemical activation process.

Fig. 3b illustrates the effect of initial MRP concentration (5–100 mg dm^{-3}) on removal efficiency. While BC showed a moderate increase in removal with concentration (from 27 % to 54 %), BCA maintained significantly higher performance (86 %–82 %) over the same range. This indicates that BCA possesses a larger number of high-affinity adsorption sites and a greater tolerance to increasing pollutant load, with an optimal adsorbent mass of 0.1 g (5 g dm^{-3}) yielding the highest removal (88 %), while already demonstrating excellent performance (85 %) at 0.05 g (2.5 g dm^{-3}).

Subsequent experiments focused solely on BCA. Fig. 4a shows that adsorption capacity increased with higher MRP concentrations, reaching approximately 80 mg g^{-1} at 100 mg dm^{-3}, while removal efficiency remained above 80 %, suggesting that active sites were not saturated under the tested conditions. Fig. 4b demonstrates that increasing BCA dosage (0.25–4 g dm^{-3}) improved removal from 79 % to 92 %, consistent with a greater availability of adsorption sites (Jha et al., 2023; Wang et al., 2024).

The effect of solution pH on MRP removal by BCA is shown in Fig. 4c. Maximum adsorption occurred at pH 3 (77 %) and decreased sharply at pH 5 (~5 %), coinciding with the isoelectric point of MRP (pI ≈ 5.15). Removal efficiency partially recovered at pH 7–11 (50–65 %), reflecting changes in electrostatic interactions between the biochar surface and MRP species. MRP has $pKa_1 = 2.9$ (carboxyl group) and $pKa_2 = 7.4$ (pyrrolidinyl amino group), giving an isoelectric point (pI) of 5.15 (AstraZeneca, 2023). Below pH 2.9, it is cationic; between 2.9 and 7.4, it exists as a zwitterion, and above pH 7.4, it is an anion. Its Log P ≤ −3.0 indicates that its aqueous solubility is essentially pH-independent. These outcomes are consistent with the pH_{PZC} of BCA (Fig. 4d), indicating that pH strongly modulates the adsorbent-adsorbate interaction. Both MRP and BCA bear positive charges at low pH (pH < pI); nonetheless, strong hydrogen bonding and π–π interactions facilitate adsorption. Near pH 5 (≈pI), MRP exists predominantly in its zwitterionic form, leading to electrostatic repulsion and a marked decline in removal efficiency. As the pH increases beyond the BCA pH_{PZC}, the surface acquires a negative charge, which favors electrostatic attraction with protonated amine groups of MRP, thereby restoring adsorption to levels of 50–65 %. These results highlight the pivotal role of pH-modulated electrostatic interactions in governing MRP adsorption, being 3 the optimal pH value.

As shown in Fig. 2a, NaOH activation markedly altered the biochar surface, creating additional functional groups that enhance MRP adsorption by BCA. Whereas raw BC exhibited two points of zero charge near pH 2 and 12, BCA displayed an extra neutrality region around pH 8 and an overall lower surface charge (Fig. 4d). These surface modifications enable strong interactions with meropenem across both acidic and alkaline conditions: Its secondary amino group remains protonated at pH ≤ 5.4, promoting n-π interactions and H-bonding (Liu et al., 2023). In contrast, it can interact with newly exposed aldehyde and ketone groups on the biochar at higher pH. This dual-mode binding accounts for the elevated removal efficiencies observed at pH 3 and between pH 7–11 and explains the pronounced drop in removal at pH 5 (Henrique et al., 2020).

It is acknowledged that the adsorbent dosages used in this study (up to 5 g dm^{-3}) are relatively high compared to typical values adopted in large-scale continuous systems. However, such levels are commonly employed in batch adsorption studies to ensure reliable removal efficiency quantification and capture kinetic and equilibrium profiles under controlled conditions. Notably, high removal (>79 %) was also achieved at much lower dosages (0.25 g dm^{-3}), indicating strong adsorption capacity even at reduced solid loading. These results provide a solid foundation for subsequent scale-up using fixed-bed columns or continuous-flow systems, in which process optimization can reduce adsorbent consumption while maintaining high performance. Similar dosages have been reported for biochar-based materials that remove antibiotics from aqueous matrices (dos Santos et al., 2019).

3.3. Kinetics, equilibrium, and thermodynamics

Kinetic and isotherm modeling are essential to understand the adsorption mechanism and evaluate the interaction dynamics between MRP and the biochar surface. Kinetic models provide insights into the rate-controlling steps, while equilibrium models describe the nature of the adsorption surface and its capacity. Thermodynamic analysis further reveals the feasibility and spontaneity of the process under different conditions.

Kinetic experiments were conducted with three initial MRP concentrations (5, 50, and 100 mg dm^{-3}) using 5.0 g dm^{-3} of BCA in ultrapure water and simulated hospital wastewater (HWW). Experimental data were fitted to the pseudo-first-order (PFO) and pseudo-second-order (PSO) models. Results are plotted in Fig. 5. The PSO model

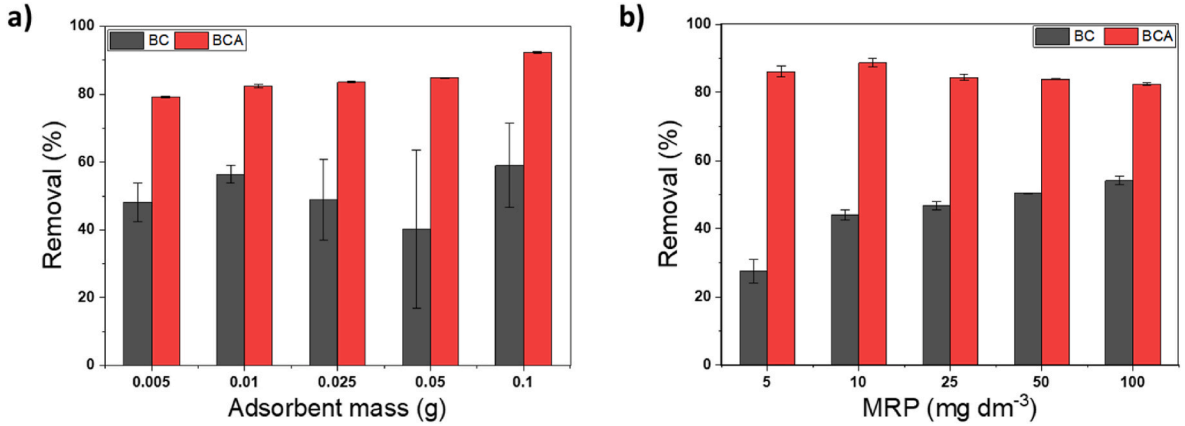

Fig. 3. – Preliminary tests using Biochar (BC) and Biochar Activated (BCA) evaluating the effect of adsorbent mass (a) and MRP initial concentration (b). Conditions: MRP initial concentration 5 mg dm^{-3}; natural pH (~7.5); 24 h of contact time; adsorbent mass 0.01 g.

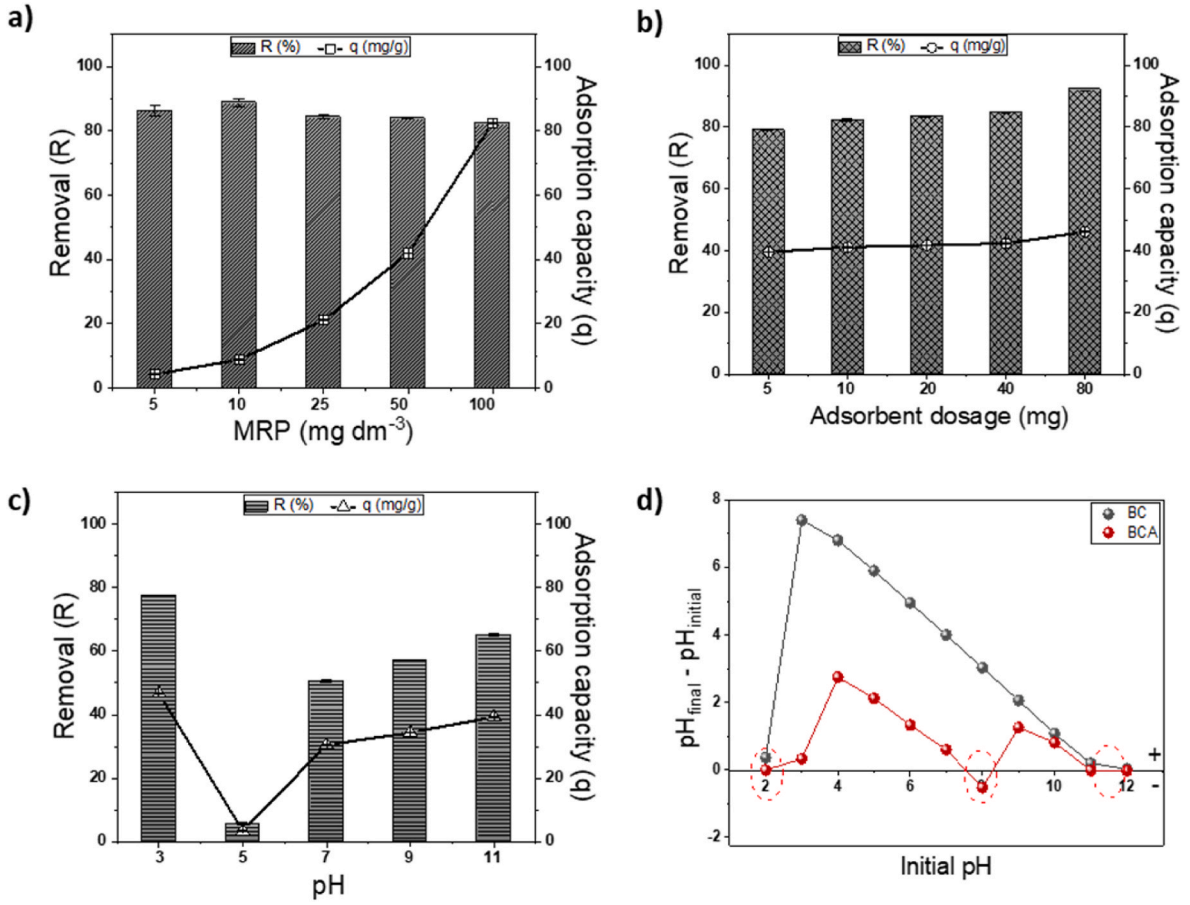

Fig. 4. – (A) Removal of different concentrations of MRP (1.0 g dm^{-3} of adsorbent). (B) Adsorbent dosage study ($[MRP]_0$: 50 mg dm^{-3}). (C) MRP removal at different pHs. (D) pH_{PZC} (1.0 g dm^{-3} of adsorbent, 24 h of contact time, and 50 mg dm^{-3} of MRP).

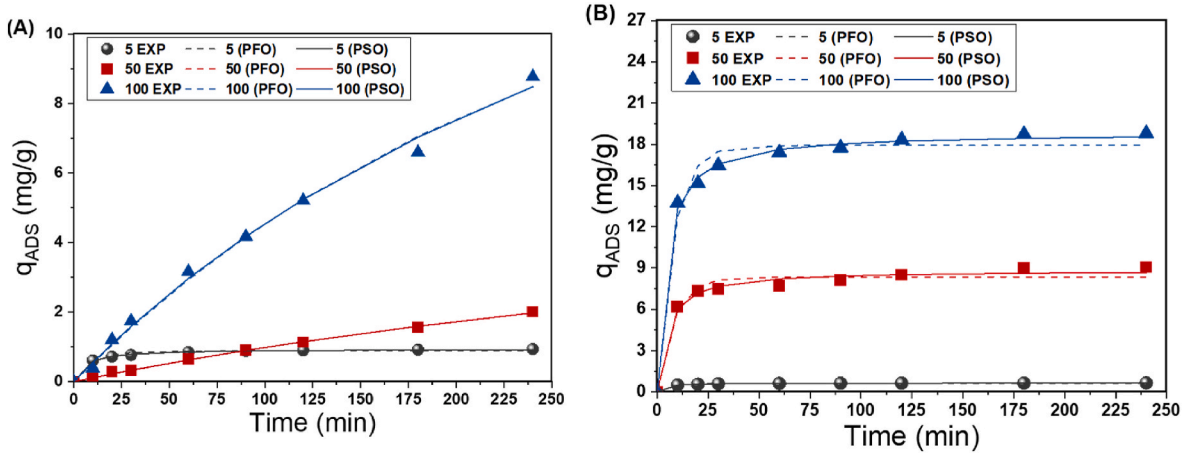

Fig. 5. – Experimental data (EXP) and kinetic fit of pseudo-first order (PFO) and pseudo-second-order (PSO) for experiments conducted using ultrapure water (a) and HWW (b).

provided a better fit in both media, with higher correlation coefficients and better agreement between calculated and experimental equilibrium capacities. For instance, in HWW at 50 mg dm^{-3}, the experimental and predicted q_e values were 18.79 and 18.86 mg g^{-1}, respectively, supporting chemisorption as the likely dominant mechanism.

In ultrapure water, equilibrium was achieved within 20 min for 5 and 50 mg dm^{-3}. At 100 mg dm^{-3}, equilibrium was not fully reached, indicating slower adsorption at higher concentrations (Fig. 5a). In contrast, in HWW, adsorption was rapid across all concentrations, suggesting that the presence of ionic species may facilitate the initial uptake (Fig. 5b).

Table 1 summarizes the Langmuir and Freundlich isotherm parameters for MRP adsorption onto BCA. Fig. 6a, c, and 6e depict the adsorption data and model fits in ultrapure water, while Fig. 6b, d, and 6f present the corresponding results for HWW.

Equilibrium isotherms were determined at 30, 45, and 60 °C over a concentration range of 5–200 mg dm^{-3}. The Freundlich model consistently showed the best fit for both ultrapure water and HWW,

Table 1
Parameters from adsorption kinetic, equilibrium and thermodynamic studies using BCA.

Models	Parameters	Ultrapure water			HWW		
		5 mg dm^{-3}	**50 mg dm^{-3}**	**100 mg dm^{-3}**	**5 mg dm^{-3}**	**50 mg dm^{-3}**	**100 mg dm^{-3}**
PFO	K_1 (min^{-1})	0.09854	0.00278	0.00402	0.14196	0.12125	0.12423
	q_e (mg.g^{-1})	0.88576	4.05839	13.69914	0.6306	8.34472	17.91608
	R^2	0.97934	0.99766	0.9931	0.98964	0.96793	0.98037
	χ^2	0.00224	0.00125	0.06127	5.12744E-4	0.28448	0.78903
PSO	K_2 (g.mg^{-1}.min^{-1})	0.1825	2.34641E-4	1.14476E-4	0.46404	0.02454	0.01274
	q_e (mg.g^{-1})	0.94287	6.99321	22.31991	0.65799	8.84467	18.86059
	R^2	0.99774	0.99758	0.99392	0.99911	0.98881	0.99754
	χ^2	1.95884E-4	0.00114	0.05402	4.42402E-5	0.09926	0.099
Models	***Parameters***	***30 °C***	***45 °C***	***60 °C***	***30 °C***	***45 °C***	***60 °C***
Langmuir	Q_m (mg.g^{-1})	152,901	592.89823	59.07287	93,956.49676	411,013.0992	903,474.5829
	K_L (L.mg^{-1})	7.32574E-6	0.00149	0.02108	4.07715E-6	1.58358E-6	2.17825E-6
	R^2	0.84521	0.99224	0.99372	0.99769	0.98985	0.97119
	χ^2	41.3342	1.73481	1.2226	0.1953	1.38832	7.12599
Freundlich	K_F [(mg.L^{-1})(L.g^{-1})1/n]	0.00245	1.08705	2.42176	0.32152	0.35265	0.84507
	n	0.33564	1.07979	1.54458	0.95508	0.84773	0.7518
	R^2	0.95154	0.99346	0.9976	0.9984	0.9979	0.9962
	χ^2	12.93933	1.46181	0.46743	0.13547	0.28336	0.93914
Liu	Q_m (mg.g^{-1})	1044.41	333.1501	43.993	40.3736	322.632	79.333
	K_{LIU} (L mg^{-1})	0.0069	0.0023	0.0293	0.01778	0.00389	0.0471
	n_{LIU}	2.1175	1.0026	1.1149	1.43602	1.3553	1.6581
	R^2	0.8338	0.9477	0.9247	0.9959	0.9551	0.9841
	χ^2	66.5676	17.5325	5.2644	0.1260	9.2063	5.8912
Sips	Q_m (mg.g^{-1})	1777.34	175.049	42.337	25.4682	98.7919	81.0763
	K_{SIPS} (L mg^{-1})	0.00809	0.00208	0.0527	0.03135	0.01241	0.0519
	n_{SIPS}	2.5200	0.7983	0.9636	1.7726	1.3976	1.8058
	R^2	0.9308	0.7733	0.8513	0.9846	0.9978	0.9976
	χ^2	27.6888	76.0100	10.398	0.4820	0.4113	0.8727
Thermo	***Parameters***	***303.15***	***318.15***	***333.15***	***303.15***	***318.15***	***333.15***
	lnK	−6.01167	0.08347	0.88449	−1.1347	−1.04228	−0.16834
	ΔG° (kJ mol^{-1})	−182.016	−191.02	−200.030	−234.66	−246.28	−257.91
	ΔH° (kJ mol^{-1})	19.51			26.67		
	ΔS° (kJ mol^{-1} K^{-1})	600.48			77.49		

demonstrated by high correlation coefficients (R^2) ranging from 0.95154 to 0.9976 across all tested temperatures (30, 45, and 60 °C). The Freundlich constant, K_f, varied between 0.00245 and 2.42176 (mg/g)(L/mg)$^{(1/n)}$, reflecting the adsorption capacity of BCA for MRP under different conditions. The Freundlich exponent, n, varied from 0.33564 at 30 °C to 1.54458 at 60 °C. Specifically, n values greater than 1 (1.07979 at 45 °C and 1.54458 at 60 °C) indicate favorable adsorption at these higher temperatures. However, at 30 °C, the n value of 0.33564 (less than 1) suggests a different adsorption behavior or less favorable conditions. Overall, the strong and consistent fit of the Freundlich model indicates heterogeneous surface adsorption with multilayer interactions, which aligns with the complex structure and varied active sites of BCA. In comparison, the Langmuir, Liu, and Sips models were also evaluated but consistently provided lower correlation coefficients, further supporting the applicability of the Freundlich model for this adsorption system (Freundlich, 1906; Sepúlveda et al., 2021).

Temperature effects revealed contrasting behavior between matrices. In ultrapure water, increasing temperature slightly reduced adsorption capacity, consistent with exothermic interactions or weak physisorption (Hameed et al., 2020; Wang et al., 2024). However, in HWW, adsorption improved with temperature, likely due to enhanced diffusion and disruption of hydration shells around MRP and the adsorbent, facilitating stronger interactions (Qiu et al., 2022).

Thermodynamic parameters confirmed the spontaneous nature of the process, with negative ΔG° values at all temperatures (Fig. 6g and h. Table 1). The positive ΔH° values indicated endothermic adsorption, particularly in HWW, while positive ΔS° values reflected increased randomness at the solid-liquid interface, possibly due to desolvation effects and rearrangement of water molecules during MRP binding (Ambaye et al., 2021).

These results confirm that BCA interacts favorably with MRP through chemisorption on heterogeneous surfaces, with performance influenced by solution chemistry and temperature. The kinetic and equilibrium modeling supports the applicability of BCA in dynamic systems and under realistic environmental conditions.

3.4. Desorption-reusability and HWW matrix study

Reusability is a key criterion for evaluating adsorbent viability at scale. To assess the economic feasibility of the adsorption process, desorption experiments were performed with 0.1 M NaOH to regenerate BCA and gauge its performance over multiple adsorption-desorption cycles. Although typical MRP concentrations in HWW are around 5 mg dm^{-3}, 50 mg dm^{-3} were employed to simulate cumulative exposure to contaminated water. After the first adsorption cycle, removal efficiencies reached 99 % in HWW and 85 % in ultrapure water (Fig. 7a). Desorption solutions were analyzed to quantify MRP recovery, and a second adsorption run, omitting regeneration, was carried out to isolate the effects of NaOH treatment on the BCA structure. A gradual decline in adsorption capacity over successive cycles suggests that repeated alkaline regeneration induces structural changes in the biochar (Jang and Kan, 2019).

After four consecutive adsorption-desorption cycles, removal efficiencies for both matrices remained remarkably stable, declining by only 1 % per cycle. In the first regeneration step, 0.1 M NaOH successfully desorbed 38 mg dm^{-3} of MRP from saturated BCA. By the fifth cycle, MRP removal still reached 90 % in HWW and 73 % in ultrapure water. The gradual decrease in adsorption capacity likely reflects a loss of active sites caused by repeated alkaline treatment. A control experiment, where BCA was reused without NaOH regeneration, removed just 24.6 % of MRP (50 mg dm^{-3}), compared to 98.5 % removal by regenerated BCA. These results underscore the effectiveness and durability of NaOH-activated biochar for multiple reuse cycles, highlighting its promise for real-world wastewater treatment.

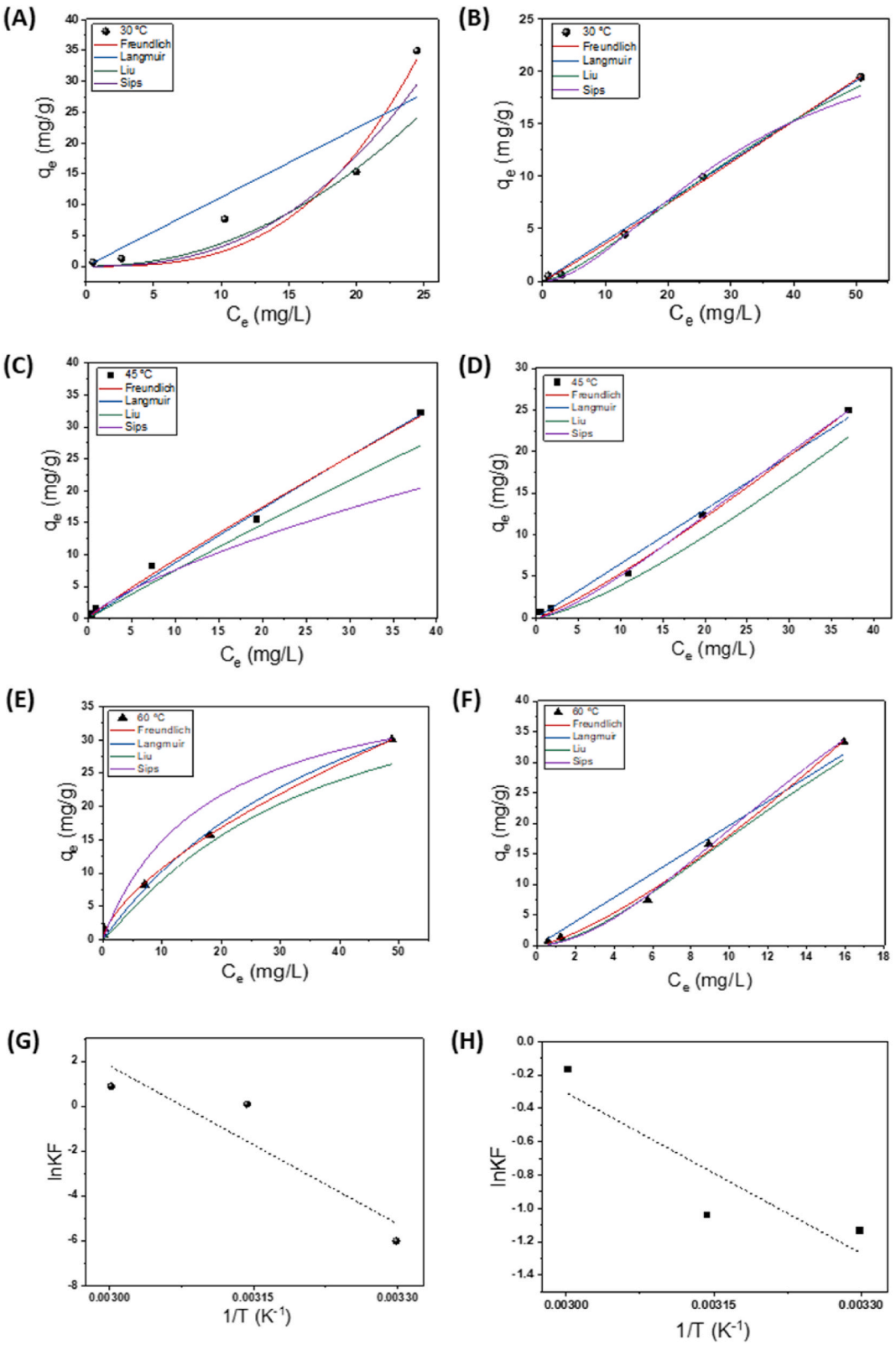

Fig. 6. – Isotherms in ultrapure water with 30 °C (a), 45 °C (c) and 60 °C (e). Isotherms in HWW with 30 °C (b), 45 °C (d), and 60 °C (f). Plot of Van't Hoff equation (g) ultrapure water; (h) HWW.

To evaluate the performance of BCA in realistic scenarios, MRP removal was compared in ultrapure water and a simulated HWW matrix. As shown in Fig. 7b, removal in HWW remained exceptionally high (99–100 %) across all tested MRP concentrations (5–100 mg dm^{-3}). In contrast, removal in ultrapure water declined modestly from 86 % at 5 mg dm^{-3} to 82 % at 100 mg dm^{-3}. Fig. 7c demonstrates that BCA also reduced the salinity of HWW at each MRP level, with significant uptake of Na^+, SO_4^{2-}, PO_4^{3-}, Cl^-, and CH_3COO^-, and corresponding adsorption

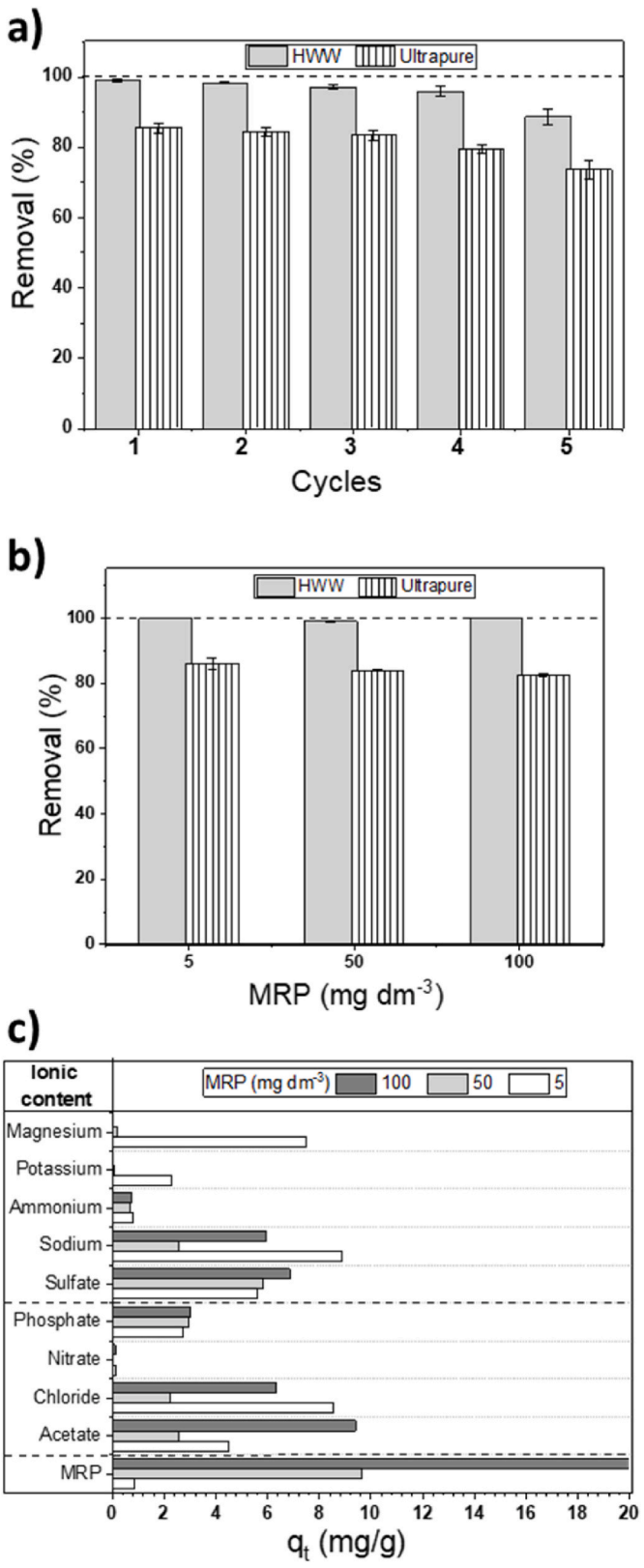

Fig. 7. – Percentage removal of MRP-50 mg dm^{-3} in reuse cycles, using 0.1 g of BCA, after 24 h of contact (a). Removal percentage of different concentrations of MRP in ultrapure water and hospital wastewater (HWW) (b). Effect of initial MRP concentration on the ionic removal from HWW (c).

capacities increasing slightly with higher MRP loads. Salinity reduction is crucial for improving effluent quality and expanding reuse options.

The superior adsorption of MRP and concomitant ion removal in saline versus ultrapure water can be explained by several synergistic mechanisms. Dissolved ions alter the biochar surface charge and the ionization state of MRP, strengthening electrostatic attractions. High ionic strength reduces antibiotic solubility, driving MRP to partition onto the biochar surface (the salting-out effect). Certain ions can form bridges between BCA functional groups and MRP or modify surface properties to enhance adsorption. Furthermore, once antibiotics occupy BCA adsorption sites, their opposite charges attract counter-ions, which hinders smaller competing species from displacing the bound molecules, thereby preserving removal efficiency (Ambaye et al., 2021; Dong et al., 2023).

It should be noted that the reusability tests conducted in this study were limited to five adsorption-desorption cycles, consistent with similar approaches in the literature (Jang and Kan, 2019). While these results demonstrate the promising potential and stability of the NaOH-activated biochar for multiple reuse cycles, longer-term studies encompassing more cycles are necessary to fully assess the durability and practical lifespan of the adsorbent under operational conditions. Future work should aim to extend these investigations to simulate real-world application scenarios better.

3.5. *Proposed adsorption mechanism*

Proposing a plausible adsorption mechanism is key to understanding MRP removal. This mechanism involves a complex combination of physical and chemical interactions between MRP and BCA, which will be detailed below. Fig. 8 schematically depicts how MRP interacts with the surface and internal pores of BCA, informed by FTIR spectra before and after adsorption. SEM images reveal a honeycomb-like network of macropores that facilitates a primary pore-filling mechanism. Activation further cleans the surface and introduces abundant functional groups, increasing adsorption sites and interaction possibilities.

Experimental data indicate that both physical and chemical forces govern adsorption. One of the cornerstones of the mechanism is electrostatic interaction, playing a central role: the high removal efficiency across varying pH values reflects the alignment of BCA point zero charge with MRP amphoteric functional groups (pK_a values of 2.9 and 7.4), enabling attraction in distinct pH regimes. This occurs because, depending on the pH of the medium, both BCA and MRP can acquire complementary surface charges (positive or negative), promoting strong mutual attraction. In addition, the mechanism is complemented by electron-donor-acceptor (EDA) interactions, such as π-π stacking between aromatic rings and n-π interactions, occur between electron-rich sites on BCA and electron-deficient moieties on MRP (Akkari et al., 2023; Ghosh and Sahu, 2023; Shaban et al., 2020).

FTIR analysis confirms that BCA surfaces are rich in oxygen and nitrogen-containing functional groups and silicon oxides, all capable of forming hydrogen bonds with MRP. It is important to note that hydrogen bonding, being a type of EDA interaction, contributes significantly to physisorption. Adsorption induces shifts in peak intensities, consistent with the occupation of multiple binding sites and supporting the Freundlich isotherm model. The coexistence of electron-rich and electron-poor regions on BCA and MRP further enhances the synergy of the EDA mechanism, including hydrogen bonding (Fig. 8). In summary, the adsorption mechanism of MRP onto BCA is governed by a robust combination of physisorption and chemisorption, orchestrated by pore-filling, electrostatic, EDA, and hydrogen bonding interactions. These combined physisorption and chemisorption processes and the material demonstrated reusability and performance in complex matrices underscore BCA promise for HWW treatment (Zeghioud and Mouhamadou, 2023).

These findings are consistent with previously reported adsorption behaviors of antibiotics on biochar-based materials (Duarte et al., 2025),

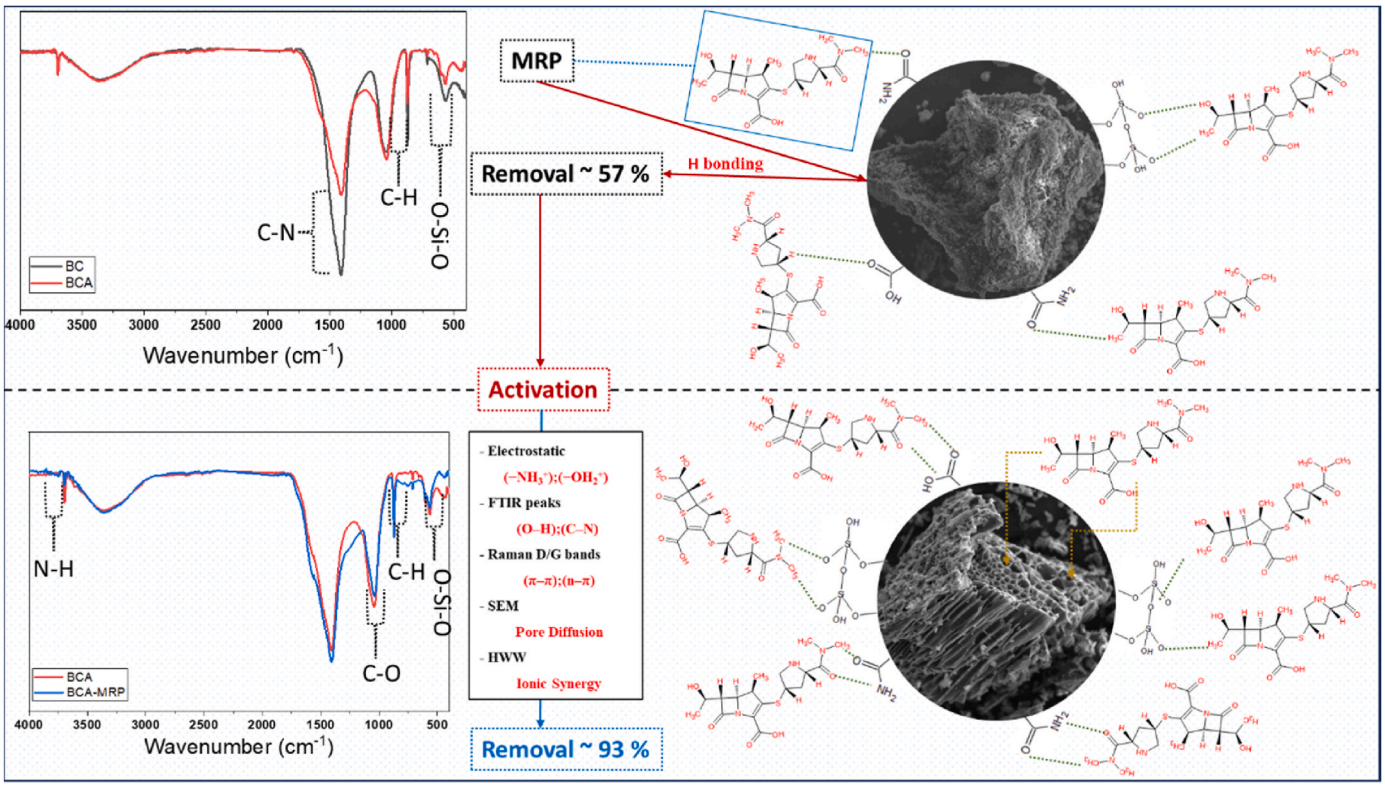

Fig. 8. – FTIR plotting of BC, BCA, and BCA-MRP with the suggested adsorption mechanism before and after activation.

and collectively illustrate the synergistic interplay between surface chemistry, porosity, and solution chemistry in governing MRP removal. This comprehensive mechanistic understanding not only supports the experimental results observed across diverse conditions but also highlights the practical applicability of BCA in realistic treatment scenarios.

4. Conclusions

This study demonstrated that NaOH-activated grape stalk biochar (BCA) is a highly effective and reusable adsorbent for removing the antibiotic meropenem (MRP) from aqueous water matrices. Activation markedly altered biochar surface properties: SEM images confirmed cleaner surfaces and more accessible pores. FTIR and Raman spectra detected new and modified functional groups. BCA achieved complete MRP removal in batch experiments, even at concentrations up to 100 mg dm^{-3}, in both simple and complex matrices. A pseudo-second-order model best described kinetic data, while equilibrium behavior followed the Freundlich isotherm. Thermodynamic parameters indicated that adsorption was endothermic in all matrices and spontaneous in both ultrapure water and hospital wastewater (HWW), an overall increase in system disorder. The adsorption mechanism involves a combination of electrostatic interactions, hydrogen bonding, and electron donor–acceptor (EDA) interactions, supported by surface functional groups introduced during activation. These interactions, together with a pore-filling effect facilitated by the honeycomb structure of the biochar, enable efficient and stable adsorption.

Long-term usability tests demonstrated that BCA retained over 90 % of its removal capacity in HWW and 73 % in ultrapure water after five successive cycles. Furthermore, BCA contributed to salinity reduction, enhancing overall water quality and pollutant uptake. FTIR analyses of used biochar confirmed specific interactions between MRP molecules and surface functional groups, underscoring the material strong affinity for the antibiotic. These findings highlight the potential of BCA as a sustainable material for treating hospital effluents contaminated with antibiotics.

CRediT authorship contribution statement

José L.S. Duarte: Writing – review & editing, Writing – original draft, Methodology, Investigation, Funding acquisition, Formal analysis, Data curation. **Ana Hayat:** Writing – review & editing, Writing – original draft, Investigation. **Mario de la Fuente:** Writing – review & editing, Resources. **Carmen M. Domínguez:** Writing – review & editing, Funding acquisition, Formal analysis, Data curation. **Aurora Santos:** Writing – review & editing, Funding acquisition. **Salvador Cotillas:** Writing – review & editing, Writing – original draft, Visualization, Validation, Supervision, Project administration, Methodology, Funding acquisition, Data curation, Conceptualization.

Declaration of competing interest

The authors declare that they have no known competing financial interests or personal relationships that could have appeared to influence the work reported in this paper.

Acknowledgments

This research is part of the grant CNS2022-135764 funded by MCIN/AEI/10.13039/501100011033 and by the European Union NextGenerationEU/PRTR, and the project PID2022-137828OB-I00 funded by MICIU/AEI/10.13039/501100011033 and by ERDF/EU. Project TEC-2024/ECO-69 (CARESOIL-CM), funded by the Community of Madrid, is also acknowledged. Dr. José Leandro da Silva Duarte acknowledges the funding received through the Marie Skłodowska-Curie grant n° 847635 of the H2020 program (UNA4CAREER) and the César Nombela grant 2023-T1/ECO-29390 of the Talent Attraction program from Community of Madrid.

Appendix A. Supplementary data

Supplementary data to this article can be found online at https://doi.

org/10.1016/j.jenvman.2025.127004.

Data availability

Data will be made available on request.

References

Ahmadi, A., Vogler, B., Deng, Y., Wu, T., 2020. Removal of meropenem from environmental matrices by electrochemical oxidation using Co/Bi/TiO2nanotube electrodes. Environ. Sci. Water Res. Technol. 6, 2197–2208.

Akkari, I., Graba, Z., Pazos, M., Bezzi, N., Manseri, A., Derkaoui, K., Kaci, M.M., 2023. NaOH-activated pomegranate Peel Hydrochar: preparation, characterization and improved acebutolol adsorption. Water Air Soil Pollut. 234.

Al Aukidy, M., Al Chalabi, S., Verlicchi, P., 2018. Hospital wastewater treatments adopted in Asia, Africa, and Australia. Handb Environ Chem. Springer Verlag 171–188.

Ambaye, T.G., Vaccari, M., van Hullebusch, E.D., Amrane, A., Rtimi, S., 2021. Mechanisms and adsorption capacities of biochar for the removal of organic and inorganic pollutants from industrial wastewater. Int. J. Environ. Sci. Technol. 18, 3273–3294.

AstraZeneca, 2023. Meropenem Environmental Risk Assessment Data.

Bhatnagar, A., Sillanpää, M., 2010. Utilization of agro-industrial and municipal waste materials as potential adsorbents for water treatment—A review. Chem. Eng. J. 157, 277–296.

Bulgariu, L., Escudero, L.B., Bello, O.S., Iqbal, M., Nisar, J., Adegoke, K.A., Alakhras, F., Kornaros, M., Anastopoulos, I., 2019. The utilization of leaf-based adsorbents for dyes removal: a review. J. Mol. Liq. 276, 728–747.

Cotillas, S., Lacasa, E., Sáez, C., Cañizares, P., Rodrigo, M.A., 2018. Disinfection of urine by conductive-diamond electrochemical oxidation. Appl. Catal. B Environ. 229, 63–70.

Crini, G., Lichtfouse, E., 2019. Advantages and disadvantages of techniques used for wastewater treatment. Environ. Chem. Lett. 17, 145–155.

da Silva, C.M.S., da Boit Martinello, K., Lütke, S.F., Godinho, M., Perondi, D., Silva, L.F. O., Dotto, G.L., 2024. Pyrolysis of grape bagasse to produce char for Cu(II) adsorption: a circular economy perspective. Biomass Convers. Biorefinery 14, 3947–3964.

da Silva Santos, D.H., Paulino, J.C.P.L., dos Santos Alves, G.F., de Magalhães Oliveira, L. M.T., de Carvalho Nagliate, P., da Silva Duarte, J.L., Meili, L., Tonholo, J., Zanta, C. L., 2021. Effluent treatment using activated carbon adsorbents: a bibliometric analysis of recent literature. Environ. Sci. Pollut. Res. 28, 32224–32235.

Dong, M., He, L., Jiang, M., Zhu, Y., Wang, J., Gustave, W., Wang, S., Deng, Y., Zhang, X., Wang, Z., 2023. Biochar for the removal of emerging pollutants from aquatic systems: a review. Int. J. Environ. Res. Publ. Health 20, 1679.

dos Santos, K.J.L., de Souza dos Santos, G.E., de Sá, Í.M.G.L., de Carvalho, S.H.V., Soletti, J.I., Meili, L., da Silva Duarte, J.L., Bispo, M.D., Dotto, G.L., 2019. Syagrus oleracea–activated carbon prepared by vacuum pyrolysis for methylene blue adsorption. Environ. Sci. Pollut. Res. 26, 16470–16481.

Duarte, J.L.S., Hayat, A., Domínguez, C.M., Santos, A., Cotillas, S., 2025. Forest biomass derived biochar for effective meropenem mitigation in hospital effluents. J. Hazard. Mater. Adv. 19, 100811.

Freundlich, H.M.F., 1906. Over the adsorption in solution. J. Phys. Chem. 57, 1100–1107.

Georgin, J., Netto, M.S., Franco, D.S.P., Piccilli, D.G.A., da Boit Martinello, K., Silva, L.F. O., Foletto, E.L., Dotto, G.L., 2022. Woody residues of the grape production chain as an alternative precursor of high porous activated carbon with remarkable performance for naproxen uptake from water. Environ. Sci. Pollut. Res. 29, 16988–17000.

Ghosh, S., Sahu, M., 2023. Adsorptive removal of dimethyl phthalate using peanut shell-derived biochar from aqueous solutions: equilibrium, kinetics, and mechanistic studies. Environ. Sci. Pollut. Res. 30, 87599–87612.

Hai Nguyen Tran, H.N.T., You ShengJie, Y.S., Hosseini-Bandegharaei, A., Chao HuanPing, C.H., 2017. Mistakes and Inconsistencies Regarding Adsorption of Contaminants from Aqueous Solutions: a Critical Review.

Hameed, R., Lei, C., Lin, D., 2020. Adsorption of organic contaminants on biochar colloids: effects of pyrolysis temperature and particle size. Environ. Sci. Pollut. Res. 27, 18412–18422.

Hayat, A., Duarte, J.L.S., Cruz-Gómez, F., Domínguez, C.M., Santos, A., Cotillas, S., 2025. Electrochemical degradation of levofloxacin in synthetic hospital effluents: insights into operating parameters, by-products formation and toxicity. Electrochim. Acta 530.

Henrique, D.C., Quintela, D.U., Ide, A.H., Erto, A., Duarte, J.L.D.S., Meili, L., 2020. Calcined Mytella falcata shells as alternative adsorbent for efficient removal of rifampicin antibiotic from aqueous solutions. J. Environ. Chem. Eng. 8.

Herraiz-Carboné, M., Lacasa, E., Cotillas, S., Vasileva, M., Cañizares, P., Rodrigo, M.A., Sáez, C., 2021. The role of chloramines on the electrodisinfection of Klebsiella pneumoniae in hospital urines. Chem. Eng. J. 409.

Ho, Y.S., McKay, G., 1999. Pseudo-second order model for sorption processes. Process Biochem. 34, 451–465.

Jang, H.M., Kan, E., 2019. A novel hay-derived biochar for removal of tetracyclines in water. Bioresour. Technol. 274, 162–172.

Jha, S., Gaur, R., Shahabuddin, S., Tyagi, I., 2023. Biochar as sustainable alternative and green adsorbent for the remediation of noxious pollutants: a comprehensive review. Toxics 11, 117.

Kordestani, B., Takdastan, A., Jalilzadeh Yengejeh, R., Neisi, A.K., 2020. Photo-Fenton oxidative of pharmaceutical wastewater containing meropenem and ceftriaxone antibiotics: influential factors, feasibility, and biodegradability studies. Toxin Rev. 39, 292–302.

Lagergren, S., 1898. About the Theory of So-Called Adsorption of Soluble Substances.

Langmuir, I., 1918. The adsorption of gases on plane surfaces of glass, mica and platinum. J. Am. Chem. Soc. 40, 1361–1403.

Lee, S.P., 2008. Synthesis and characterization of carbon nitride films for micro humidity sensors. Sensors 8, 1508–1518.

Liu, T., Chen, L., Yu, P., Li, Q., Lou, J., 2023. Development and validation of a strong cation exchange chromatographic column coupled with high-performance liquid chromatography method for Meropenem and evaluation of its stability in human plasma: application to the therapeutic drug monitoring. J. Chromatogr. Sci. 61, 656–664.

Liu, Y., Xu, H., Yang, S.-F., Tay, J.-H., 2003. A general model for biosorption of Cd2+, Cu2+ and Zn2+ by aerobic granules. J. Biotechnol. 102, 233–239.

Lucaci, A.R., Bulgariu, D., Ahmad, I., Lisă, G., Mocanu, A.M., Bulgariu, L., 2019. Potential use of biochar from various waste biomass as biosorbent in Co(II) removal processes. Water 11, 1565.

Majumdar, A., Das, S.C., Shripathi, T., Hippler, R., 2012. Chemical synthesis and surface morphology of amorphous hydrogenated carbon nitride film deposited by N2/CH4 dielectric barrier discharge plasma. Compos. Interfaces 19, 161–170.

Moratalla, A., Cotillas, S., Lacasa, E., Fernández-Marchante, C.M., Ruiz, S., Valladolid, A., Cañizares, P., Rodrigo, M.A., Sáez, C., 2022. Occurrence and toxicity impact of pharmaceuticals in hospital effluents: simulation based on a case of study. Process Saf. Environ. Prot. 168, 10–21.

Pham, T.N.M., Hoang, T.H., Nguyen, T.P., Nguyen, Q.K., Pham, B., Hoang, Q.A., Pham, T.D., Nguyen, T.A.H., Le, A.T., Pham, D.T., 2022. Adsorption characteristics of antibiotic Meropenem on magnetic CoFe2O4@Au nanoparticles. Adsorpt. Sci. Technol. 2022.

Qiu, M., Liu, L., Ling, Q., Cai, Y., Yu, S., Wang, S., Fu, D., Hu, B., Wang, X., 2022. Biochar for the removal of contaminants from soil and water: a review. Biochar 4, 19.

Sepúlveda, P., Erto, A., Duarte, J.L.d.S., Meili, L., 2021. Fundamentals of adsorption in liquid phase. In: Meili, L., Dotto, G.L. (Eds.), Advanced Magnetic Adsorbents for Water Treatment: Fundamentals and New Perspectives. Springer International Publishing, Cham, pp. 1–24.

Shaban, M.A.A., Ibrahim, M.A., M-Ridha, M.J., Hussein, H.A., 2020. Adsorption of meropenem antibiotics from aqueous solutions on multi-walled carbon nanotube. Int. Rev. Civ. Eng. 11, 283–293.

Shukla, S., Khan, R., Srivastava, M.M., Zahmatkesh, S., 2024. Valorization of waste watermelon rinds as a bio-adsorbent for efficient removal of Methylene blue dye from aqueous solutions. Appl. Biochem. Biotechnol. 196, 2534–2548.

Sips, R., 1948. On the structure of a catalyst surface. J. Chem. Phys. 16, 490–495.

Vasconcelos, K.C., Alencar, S.G., Vich, D.V., Oliveira, L.M.T.M., Bernardo, V.B., da Duarte, J.L.S., 2023. Application of agricultural waste from main Brazilian crops as adsorbent for wastewater treatment. Rev. Virtual Quim. 15, 956–983.

Verlicchi, P., 2021. Trends, new insights and perspectives in the treatment of hospital effluents. Curr. Opin. Environ. Sci. Health 19.

Wang, Y., Chen, L., Zhu, Y., Fang, W., Tan, Y., He, Z., Liao, H., 2024. Research status, trends, and mechanisms of biochar adsorption for wastewater treatment: a scientometric review. Environ. Sci. Eur. 36, 25.

Zeghioud, H., Mouhamadou, S., 2023. Dye removal characteristics of magnetic biochar derived from sewage sludge: isotherm, thermodynamics, kinetics, and mechanism. Water Air Soil Pollut. 234.